The Euler Equations

Revised Notes November 1994

Thomas H. Pulliam

NASA Ames Research Center

ABSTRACT A review of material pertinent to the solution of the Euler equations will be presented. The equation sets are examined in both the continuous partial differential form and the integral form. Various properties, transformations and forms of the equations will be discussed. The eigensystem of the equations will be used extensively in developing a framework for various methods applied to the Euler equations. Perspectives to the Navier-Stokes and full potential equations are included. Applications are used to demonstrate the use of the Euler equations.

I. Introduction

The Euler equations as they're known today are comprised of the inviscid compressible continuity, momentum (originally known as the Euler equations) and in most instances the energy equations. As many know the term "Euler equations" originally denoted the inviscid momentum equations and it is only recently (possibly the last 10-15 years) that the full set of inviscid equations have been termed the "Euler equations". The Euler equations are of interest for a number of reasons. They are the next step after the potential equation in the heriarchy of equations which lead us to the full Navier-Stokes. Besides being valid for use in applications where viscous effect are neglible, they are often used in analysis and development of algorithms which eventually get applied to the Navier-Stokes equations. Since the equations are capable of capturing, convecting and creating vorticity, they are often used to simulate vortical flows where either physical mechanisms (such as shocks) or artifical mechanisms (fixed stagnation points, numerical dissipation) account for the production of vorticity. In some cases, the resulting flows represent acceptable physical solutions and in others the validity of the Euler solution is in question relative to a more physical Navier-Stokes equation solution.

It would be too time consuming to try to cover all the attempts and successes of analytic or numerical solutions to the Euler equations. Rather we will concentrate here on the mathematical and physical form of the equations. In particular, we will look at approximations (e.g. reductions using the eigensystems or thermodynamic assumptions) and particular forms (e.g. Reimann equations, flux difference/split forms).

Some limited examples will be given before closing, which serve to demonstrate the current state of the art. But as you will see we may raise more questions

1

about the application of the Euler solvers then we answer. The manuscript is not intended to be a review of Euler methods or solution techniques. I leave that to other presentations. Rather, I will hopefully give the reader a set of tools which are usually needed when developing an Euler algorithm or code.

II. Euler Equations

We shall restrict ourselves in most of the development to the Cartesian form of the two- dimensional (2-D) equations in strong conservation law form. Strong conservation law form is chosen because we wish to admit shock capturing. We shall also look at nonconservative forms and the one- dimensional (1-D) equations where appropriate. Typically the extension of ideas to three- dimensions (3-D) is rather straight-forward. It is usually a mistake to restrict oneself to just 1-D equations, since ideas developed for 1-D often are difficult to extend formally to multi- dimensions. In contrast, the extension from 2-D to 3-D is more easily accomplished.

2.1 The Euler Equations

The Euler equations in nondimensional conservation law form are

$$\partial_t Q + \partial_x E + \partial_y F = 0 \qquad (2.1-1)$$

where

$$Q = \begin{bmatrix} \rho \\ \rho u \\ \rho v \\ \epsilon \end{bmatrix}, \quad E = \begin{bmatrix} \rho u \\ \rho u^2 + p \\ \rho uv \\ u(\epsilon + p) \end{bmatrix}, \quad F = \begin{bmatrix} \rho v \\ \rho uv \\ \rho v^2 + p \\ v(\epsilon + p) \end{bmatrix} \qquad (2.1-2)$$

Pressure is related to the conservative flow variables, Q, by the equation of state

$$p = (\gamma - 1)\left(\epsilon - \frac{1}{2}\rho(u^2 + v^2)\right) \qquad (2.1-3)$$

where γ is the ratio of specific heats, generally taken as 1.4. The speed of sound is c which for ideal fluids, $c^2 = \gamma p/\rho$.

It is sometimes useful to recast the energy equation in terms of enthalpy, $h = (\epsilon + p)/\rho$

$$\partial_t \epsilon + \partial_x(\rho u h) + \partial_y(\rho v h) = 0 \qquad (2.1-4)$$

2.2 General Form

First, let us recast Eqs. (2.1) in a more general form

2

$$Q = \begin{bmatrix} q_1 \\ q_2 \\ q_3 \\ q_4 \end{bmatrix}, \quad E = \begin{bmatrix} q_2 \\ q_2^2/q_1 + p(q) \\ q_2 q_3/q_1 \\ q_2 \left(q_4 + p(q) \right)/q_1 \end{bmatrix}; \quad F = \begin{bmatrix} q_3 \\ q_2 q_3/q_1 \\ q_3^2/q_1 + p(q) \\ q_3 \left(q_4 + p(q) \right)/q_1 \end{bmatrix} \qquad (2.2-1)$$

with

$$p(q) = (\gamma - 1)(q_4 - \frac{1}{2}\left(q_2^2 + q_3^2 \right)/q_1) \qquad (2.2-2)$$

In using Eqs. (2.2) we will always assume that the q_i variables are independent of each other. This is important when we will be examining linearizations and Jacobians of the fluxes.
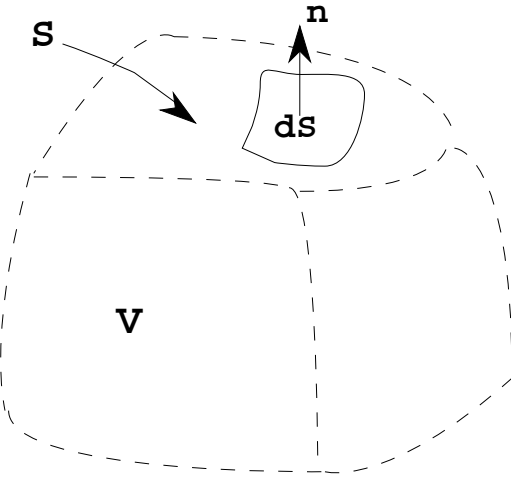

FIGURE 1. Control Volume For Fluid Flow Equations.

The above equations are the continuous partial differential form (PDF) of the Euler equations. We next digress to the integral form (IF) of the equations. Consider a control volume, as in Fig. 1, where we have a flux of some quantity (e.g. mass, momentum or energy) into and out of the volume plus the rate in time at which the quantity increases or decreses in the volume must balance to zero. This can be stated in integral form as

$$\frac{d}{dt}\int Q dV + \oint \mathbf{n} \cdot F dS = 0 \qquad (2.2-3)$$

where V is the cell volume, $\mathbf{n}dS$ is a vector element of surface area with outward normal $\mathbf{n}$ and Q, F are defined above. The integral form of the equations is often

3

used when finite volume integration schemes are developed since it leads to the natural definition of flux balances on a computational cell.

2.3 Nonconservative Form

Finally, for later use we can recast Eqs (2.1) in nonconservative form

$$\partial_t \widehat{Q} + M \partial_x \widehat{Q} + N \partial_y \widehat{Q} = 0 \qquad (2.3-1)$$

$$\widehat{Q} = \begin{bmatrix} \rho \\ u \\ v \\ p \end{bmatrix}, \quad M = \begin{bmatrix} u & \rho & 0 & 0 \\ 0 & u & 0 & \rho^{-1} \\ 0 & 0 & u & 0 \\ 0 & \gamma p & 0 & u \end{bmatrix}, \quad N = \begin{bmatrix} v & 0 & \rho & 0 \\ 0 & v & 0 & 0 \\ 0 & 0 & v & \rho^{-1} \\ 0 & 0 & \gamma p & v \end{bmatrix} \qquad (2.3-2)$$

The elements of the vector $\widehat{Q}$ are sometimes termed the primitive variables.

III. One Dimensional Forms

3.1 Conservative 1-D Euler Equations

One can reduce Eqs. (2.1) to a one dimensional form where we have

$$\partial_t Q + \partial_x E = 0 \qquad (3.1-1)$$

with

$$Q = \begin{bmatrix} \rho \\ \rho u \\ \epsilon \end{bmatrix}, \quad E = \begin{bmatrix} \rho u \\ \rho u^2 + p \\ u(\epsilon + p) \end{bmatrix} \qquad (3.1-2)$$

These equations have found a lot of use in studying the shock tube problem where a long tube is initialized with two chambers at different pressures separated by a diaphram which is subsequently removed. This results in a shock, contact discontinuity and rarefraction wave which propagate through the tube. One can then analyze a numerical technique for shock jump errors, smearing of the discontinuities, errors in wave speeds and reflection boundary conditions if multiple waves or fixed boundaries are used.

3.2 Quasi- 1-D Euler Equations

We can derive a set of quasi- one dimensional Euler equations (see e.g. Liepmann and Roshko [1] or Thompson [2]). Here we have one - dimensional flow in a nozzle with cross sectional area $\widehat{a}(x)$, the resulting equations are

4

$$\partial_t \widehat{a} Q + \partial_x \widehat{a} E + H = 0 \qquad (3.2-1)$$

with

$$H = \begin{bmatrix} 0 \\ -p\partial_x \widehat{a} \\ 0 \end{bmatrix} \qquad (3.2-2)$$

Since we have an added source term H in the quasi - one dimensional equations we can have a nontrivial steady state solution where the time derivative vanishes and the fluxes balance. A typical example is given in Fig. 2. The nozzle has $\widehat{a} = 1.398 + 0.347 \tanh(0.8x - 4)$ for $0 \leq x \leq 10$. The cases shown are for a supersonic ($M_\infty = 1.2$) inlet - subsonic outlet with a shock standing at $x \approx 5$. The density is shown for both the exact solution and numerical calculation (done using an explicit and implicit second order accurate TVD scheme, Ref. [12]).

(a) Explicit TVD method. (b) Implicit TVD method.
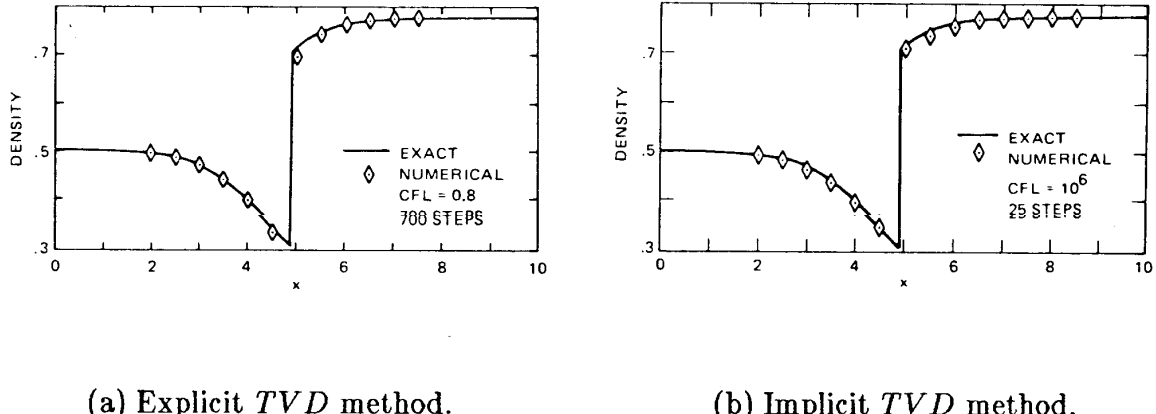
FIGURE 2.   Quasi- One Dimensional Euler Solution For Laval Nozzle.

3.3 Nonconservative 1-D Euler Equations
The 1-D form of the nonconservative equations is

$$\partial_t \widehat{Q} + M \partial_x \widehat{Q} = 0 \qquad (3.3-1)$$

$$\widehat{Q} = \begin{bmatrix} \rho \\ u \\ p \end{bmatrix}, \quad M = \begin{bmatrix} u & \rho & 0 \\ 0 & u & \rho^{-1} \\ 0 & \gamma p & u \end{bmatrix} \qquad (3.3-2)$$

IV. Jacobians, Similarity Transformations and Eigensystems

4.1 Flux Jacobians

The fluxes (e.g. E and F) defined in the previous section are nonlinear functions of Q. In stability analysis and design of numerical algorithms for the Euler equations the flux Jacobians

$$A \equiv \frac{\partial E}{\partial Q}, \quad B \equiv \frac{\partial F}{\partial Q} \qquad (4.1-1)$$

play a dominant role.

For example, if we attempt to use the 1st order implicit scheme

$$\frac{Q^{n+1} - Q^n}{\Delta t} + E(Q)^{n+1} = 0 \qquad (4.1-2)$$

to integrate Eq. (3.1) the second term is nonlinear in Q^{n+1}. We can linearize that term to 2nd order accuracy by a Taylor series expansion

$$E^{n+1} = E^n + A^n(Q^{n+1} - Q^n) + O(\Delta t^2) \qquad (4.1-3)$$

resulting in

$$[I + \Delta t \partial_x A^n](Q^{n+1} - Q^n) = -\Delta t \partial_x E^n \qquad (4.1-4)$$

which is now linear in the solution variable Q^{n+1}.

The easiest way to derive the flux Jacobians is to start with the general form of the fluxes given in Eq. (2.2). The elements of A are defined as

$$A_{i,j} = \frac{\partial E_i}{\partial q_j}$$

where the q_j are assumed to be independent of each other. For example, $E_2 = \rho u^2 + p = q_2^2/q_1 + p(q)$ and the element $A_{2,1}$ is found to be

$$A_{2,1} = \frac{\partial E_2}{\partial q_1} = -\frac{q_2^2}{q_1^2} + \frac{(\gamma-1)}{2}\left(\frac{q_2^2 + q_3^2}{q_1^2}\right) = \frac{(\gamma-1)(u^2 + v^2)}{2} - u^2$$

The Jacobian matrices for the two- dimensional Eqs. (2.1) are

$$A = \begin{bmatrix} 0 & 1 & 0 & 0 \\ \frac{(\gamma-1)(u^2+v^2)}{2} - u^2 & (3-\gamma)u & -(\gamma-1)v & (\gamma-1) \\ -uv & v & u & 0 \\ a_1 u & \frac{\gamma e}{\rho} - \frac{(\gamma-1)(u^2+v^2)}{2} - (\gamma-1)u^2 & -(\gamma-1)uv & \gamma u \end{bmatrix}$$

$$(4.1-5)$$

6

$$B = \begin{bmatrix} 0 & 0 & 1 & 0 \\ \frac{-uv}{2} & v & u & 0 \\ \frac{(\gamma-1)(u^2+v^2)}{2} - v^2 & -(\gamma-1)u & (3-\gamma)v & (\gamma-1) \\ a_1 v & -(\gamma-1)uv & \frac{\gamma e}{\rho} - \frac{(\gamma-1)(u^2+v^2)}{2} - (\gamma-1)v^2 & \gamma v \end{bmatrix}$$

$$(4.1-6)$$

with $a_1 = (\gamma-1)(u^2+v^2) - \frac{\gamma e}{\rho}$.

4.2 Homogeneous Property

The fluxes of the Euler equations have the very interesting and useful property of being homogeneous of degree 1, i.e. $E(sQ) = sE(Q)$ Since the fluxes are homogeneous of degree 1 they can be shown to satisfy $E = AQ$, , $F = BQ$ exactly. Beam and Warming took advantage of this in the original development of their implicit approximate factorization algorithm [3]. Steger and Warming [4] also used this property as an integral part of their development of a flux split algorithm (Vinokur [5] shows how to dispense with this requirement). We can use the homogeneous property here to show that, for instance,

$$\frac{\partial E}{\partial x} = \frac{\partial AQ}{\partial x} = A\frac{\partial Q}{\partial x} + \frac{\partial A}{\partial x}Q \qquad (4.2-1a)$$

also

$$\frac{\partial E}{\partial x} = \frac{\partial E}{\partial Q}\frac{\partial Q}{\partial x} = A\frac{\partial Q}{\partial x} \qquad (4.2-1b)$$

which implies that

$$\frac{\partial A}{\partial x}Q = 0 \qquad (4.2-2)$$

One can verify this by using Eqs. (2.1) and (4.1-5,6). Similar expressions hold for any derivative of E and F. Using such relations we can form the quasi- linear form of Eqs (2.1)

$$\partial_t Q + A\partial_x Q + B\partial_y Q = 0 \qquad (4.2-3)$$

4.3 Eigenvector Matrices

It is well known that the flux Jacobians A and B each have real eigenvalues and a complete set of eigenvectors. Therefore, the Jacobian matrices can be diagonalized. Warming, Beam, and Hyett [6] consider a general matrix which is a linear combination of A and B,

$$\widehat{A} = \kappa_x A + \kappa_y B \qquad (4.3-1a)$$

The diagonalization similarity transformation is

$$\Lambda_\kappa = T_\kappa^{-1}\widehat{A}T_\kappa \qquad (4.3-1b)$$

7

with T_κ the matrix whose columns are the eigenvectors of $\widehat{A}$ and T_κ^{-1} the corresponding left eigenvector matrix.

$$
\Lambda_\kappa = \begin{bmatrix} U & & & \\ & U & & \\ & & U + c\sqrt{\kappa_x^2 + \kappa_y^2} & \\ & & & U - c\sqrt{\kappa_x^2 + \kappa_y^2} \end{bmatrix} \qquad (4.3-2)
$$

$$
T_\kappa = \begin{bmatrix} 1 & 0 & 1 & 1 \\ u & \widetilde{\kappa}_y & (u + \widetilde{\kappa}_x c) & (u - \widetilde{\kappa}_x c) \\ v & -\widetilde{\kappa}_x & (v + \widetilde{\kappa}_y c) & (v - \widetilde{\kappa}_y c) \\ \frac{\phi^2}{(\gamma-1)} & (\widetilde{\kappa}_y u - \widetilde{\kappa}_x v) & \left[\frac{\phi^2+c^2}{(\gamma-1)} + c\widetilde{\theta}\right] & \left[\frac{\phi^2+c^2}{(\gamma-1)} - c\widetilde{\theta}\right] \end{bmatrix} \qquad (4.3-3)
$$

$$
T_\kappa^{-1} = \begin{bmatrix} (1 - \phi^2/c^2) & (\gamma-1)u/c^2 & (\gamma-1)v/c^2 & -(\gamma-1)/c^2 \\ -(\widetilde{\kappa}_y u - \widetilde{\kappa}_x v) & \widetilde{\kappa}_y & -\widetilde{\kappa}_x & 0 \\ \beta(\phi^2 - c\widetilde{\theta}) & \beta[\widetilde{\kappa}_x c - (\gamma-1)u] & \beta[\widetilde{\kappa}_y c - (\gamma-1)v] & \beta(\gamma-1) \\ \beta(\phi^2 + c\widetilde{\theta}) & -\beta[\widetilde{\kappa}_x c + (\gamma-1)u] & -\beta[\widetilde{\kappa}_y c + (\gamma-1)v] & \beta(\gamma-1) \end{bmatrix}
$$

$$(4.3-4)$$

with $U = \kappa_x u + \kappa_y v$, $\quad \phi^2 = \frac{1}{2}(\gamma-1)(u^2 + v^2)$, and $\beta = 1/(2c^2)$, $\widetilde{\theta} = \widetilde{\kappa}_x u + \widetilde{\kappa}_y v$, and, for example, $\widetilde{\kappa}_x = \kappa_x/\sqrt{\kappa_x^2 + \kappa_y^2}$.

We can recover the individual eigenvalue and eigenvector matrices for A and B by using $\kappa_x = 1, \kappa_y = 0$ for T_A, T_A^{-1}, Λ_A and $\kappa_x = 0, \kappa_y = 1$ for T_B, T_B^{-1}, Λ_B. An interesting relation exist between T_A and T_B of the form

$$
\widehat{N} = T_A^{-1} T_B; \quad \widehat{N}^{-1} = T_B^{-1} T_A \qquad (4.3-5)
$$

where

$$
\widehat{N} = \begin{bmatrix} 1 & 0 & 0 & 0 \\ 0 & 0 & -\mu & \mu \\ 0 & \mu & \mu^2 & \mu^2 \\ 0 & -\mu & \mu^2 & \mu^2 \end{bmatrix} \qquad \widehat{N}^{-1} = \begin{bmatrix} 1 & 0 & 0 & 0 \\ 0 & 0 & \mu & -\mu \\ 0 & -\mu & \mu^2 & \mu^2 \\ 0 & \mu & \mu^2 & \mu^2 \end{bmatrix} \qquad (4.3-6)
$$

with $\mu = 1/\sqrt{2}$.

Note that the matrix $\widehat{N}$ is not a function of the flow variables and is in fact a constant matrix.

It is not possible to simultaneously diagonalize the flux Jacobians of the Euler equations. It is possible to simultaneously symmetrize the equations which is often

8

useful in stability analysis. The eigenvector matrices T_κ and T_κ^{-1} will diagonalize one and symmetrize the other flux Jacobian matrix depending on the choice of κ_x and κ_y.

4.4 Similarity Transforms For Nonconservative Matrices

Warming, Beam and Hyett [6] and Steger[7] point out the relations between the conservative Jacobian Matrices A, B and the nonconservative matrices M, N. It is easy to show that the coefficient matrices M and N have the same eigenvalues as A and B, e.g.

$$\Lambda_A = \Lambda_M = \begin{bmatrix} u & & & \\ & u & & \\ & & u+c & \\ & & & u-c \end{bmatrix}, \qquad (4.4-1)$$

Therefore since each matrix is nondefective, i.e. they both have a complete set of eigenvectors, then M is similar to A and N is similar to B with the similarity transformation

$$A = SMS^{-1} \quad \text{and} \quad B = SNS^{-1} \qquad (4.4-2)$$

with

$$S = \begin{bmatrix} 1 & 0 & 0 & 0 \\ u & \rho & 0 & 0 \\ v & 0 & \rho & 0 \\ \frac{u^2+v^2}{2} & \rho u & \rho v & (\gamma-1)^{-1} \end{bmatrix} \qquad (4.4-3a)$$

$$S^{-1} = \begin{bmatrix} 1 & 0 & 0 & 0 \\ -u/\rho & \rho^{-1} & 0 & 0 \\ -v/\rho & 0 & \rho^{-1} & 0 \\ \frac{(\gamma-1)u^2+v^2}{2} & -(\gamma-1)u & -(\gamma-1)v & (\gamma-1) \end{bmatrix} \qquad (4.4-3b)$$

Using Eqs (4.3) and (4.4) one can obtain the eigenvector matrices for M and N by simple substitution.

For completeness, we have the 1-D similarity transforms

$$S = \begin{bmatrix} 1 & 0 & 0 \\ u & \rho & 0 \\ \frac{u^2}{2} & \rho u & (\gamma-1)^{-1} \end{bmatrix}, \quad S^{-1} = \begin{bmatrix} 1 & 0 & 0 \\ -u/\rho & \rho^{-1} & 0 \\ \frac{(\gamma-1)u^2}{2} & -(\gamma-1)u & (\gamma-1) \end{bmatrix} \qquad (4.4-4)$$

and here we give the eigenvector matrices for the 1-D M matrix

$$\widetilde{T} = \begin{bmatrix} 1 & \rho/(\sqrt{2}c) & \rho/(\sqrt{(2)}c) \\ 0 & 1/\sqrt{2} & -1/\sqrt{2} \\ 0 & \rho c/\sqrt{2} & -\rho c/\sqrt{2} \end{bmatrix}, \widetilde{T}^{-1} = \begin{bmatrix} 1 & 0 & -1/c^2 \\ 0 & 1/\sqrt{2} & 1/(\sqrt{2}\rho c) \\ 0 & -1/\sqrt{2} & 1/(\sqrt{2}\rho c) \end{bmatrix} \qquad (4.4-5)$$

9

Again, the eigenvector matrices for A can be found from the above matrices.

4.5 Representative Model Equations

The quasi- linear form Eq. (4.2-3) is often used for stability analysis. For simplicity, let us examine a one dimensional coupled system of linear equations of the form

$$Q_t + AQ_x = 0 \qquad (4.5-1)$$

where A is analogous to the flux Jacobian matrix. Here we have assumed that A is a constant matrix and that A has the complete set of real eigenvalues and eigenvectors as discussed above.

$$\Lambda = T^{-1}AT \qquad (4.5-2)$$

Multiplying Eq. (4.5-1) by T^{-1} and combining terms using Eq. (4.5-2) we have

$$T^{-1}Q_t + T^{-1}ATT^{-1}Q_x = W_t + \Lambda W_x = 0 \qquad (4.5-3)$$

with $W = T^{-1}Q$. Since A is linear and constant the eigenvector matrix T^{-1} can be brought through the derivatives.

The resulting system is now uncoupled and we can examine the representative model equation

$$w_t + \lambda w_x = 0 \qquad (4.5-4)$$

where λ represents an eigenvalue of A.

The choice of the type of difference forms to use in the space derivatives for the Euler equations can be justified by a linear stability analysis using the representative Eq. (4.5-4). We shall examine different finite difference approximations for the spatial derivative and use Fourier analysis to determine conditions on λ for stability.

If the second order central difference operator is applied to the model equation one gets

$$(w_j)_t + \lambda\left(w_{j+1} - w_{j-1}\right)/(2\Delta x) = 0 \qquad (4.5-5)$$

where j is the spatial index. This is the ODE (ordinary differential equation) approach to the analysis, since now we are dealing with a system of ODE's.

Classical Fourier analysis can be performed by assuming periodic boundary conditions and a solution of the form

$$w(x_j,t) = e^{\alpha t}e^{i\beta j\Delta x} \qquad (4.5-6)$$

with $i = \sqrt{-1}$ and $x_j = j\Delta x$.

Substituting this into Eq. (4.5-4) yields

$$\alpha e^{\alpha t}e^{i\beta j\Delta x} + \lambda\left(e^{\alpha t}e^{i\beta(j+1)\Delta x} - e^{\alpha t}e^{i\beta(j-1)\Delta x}\right)/(2\Delta x) = 0 \qquad (4.5-7)$$

10

The stability of the ODE is dependent on the sign of $\Re(\alpha)$ (the real part). Obviously, if $\Re(\alpha) > 0$ then $w(x, t)$ will grow unboundedly with time.

For Eq. (4.5-7)

$$\alpha = -\lambda \left(e^{i\beta\Delta x} - e^{-i\beta\Delta x}\right)/(2\Delta x) = -\lambda i \, \sin(\beta\Delta x)/\Delta x \qquad (4.5-8)$$

Since α is pure imaginary ($\Re(\alpha) = 0$) the scheme is stable in the ODE sense, independent of the sign of λ.

If one-sided difference formulas are employed, conditions on λ arise. For simplicity, let us consider first order one-sided differences.

Applying forward differencing to the model Eq. (4.5-4) gives

$$(w_j)_t + \lambda \left(w_{j+1} - w_j\right)/\Delta x = 0 \qquad (4.5-9)$$

Fourier analysis produces

$$\alpha + \lambda \left(e^{i\beta\Delta x} - 1\right)/\Delta x = 0 \qquad (4.5-10)$$

so that,

$$\alpha = \lambda \left(1 - e^{i\beta\Delta x}\right)/\Delta x = \lambda \left[1 - \cos\left(\beta\Delta x\right) + i\sin\left(\beta\Delta x\right)\right]/\Delta x \qquad (4.5-11)$$

Since $\cos\left(\beta\Delta x\right)$ is bounded by 1, $\Re(\alpha)$ will be less than zero if $\lambda < 0$. So for forward spatial differencing λ must be less than zero for stability. A similar argument for first order backward differencing shows that $\lambda > 0$ for stability. It can be shown that for higher order one sided differences the stability requirements on λ remain the same.

These results have a direct application to the choice of differencing for the Euler equations. If we stick with the standard form of Euler equations the actual flux Jacobians have eigenvalues (equivalent to λ) with both positive and negative signs depending on the flow conditions. For purely supersonic flow in the x coordinate direction ($u > c$), all the λ are positive and we could employ purely backward differences in that direction. But for subsonic flow ($u < c$), (in which case λ could be positive or negative), the only choice would be central differencing unless we recast the equations in other forms where terms have Jacobians with eigenvalues of one sign or the other. This is the basis for upwind techniques which are very popular today. In the next Section we will develop splitting for the Euler fluxes which are used in the development of upwind characteristic based schemes.

11

V. Flux Forms

5.1 Compatibility Equations and Riemann Invariants

The method of characteristics (see Chapter 12 of Liepmann and Roshko [1]) may be viewed as a first attempt at splitting up the fluid equations into terms or directions along which certain functions either are constant or vary in a predetermined fashion.

We can generate a set of compatibility relations from the nonconservative Euler equations by using the eigensystems defined above. Multiply the inviscid 1-D equations (3.3) by the left eigenvector matrix $\widetilde{T}^{-1}$

$$\widetilde{T}^{-1}\partial_t\widehat{Q} + \widetilde{T}^{-1}M\partial_x\widehat{Q} = 0 \qquad (5.1-1)$$

Writting out each equation in turn we have

$$\partial_t\rho - \frac{1}{c^2}\partial_t p + u\left(\partial_x\rho - \frac{1}{c^2}\partial_x p\right) \qquad (5.1-2a)$$

$$\partial_t u + \frac{1}{\rho c}\partial_t p + (u+c)\left(\partial_x u + \frac{1}{\rho c}\partial_x p\right) \qquad (5.1-2b)$$

$$\partial_t u - \frac{1}{\rho c}\partial_t p + (u-c)\left(\partial_x u - \frac{1}{\rho c}\partial_x p\right) \qquad (5.1-2c)$$

Note we have cleared a $1/\sqrt{2}$ and minus sign from the last two equations.
In the case of a perfect gas $\gamma p/\rho = c^2$ and we can rewrite Eq. (5.1-2a) as

$$\frac{\gamma}{\rho}\partial_t\rho - \frac{1}{p}\partial_t p + u\left(\frac{\gamma}{\rho}\partial_x\rho - \frac{1}{p}\partial_x p\right) \qquad (5.1-3)$$

For a perfect gas the chain rule relation between entropy s and ρ,p is (see Thompson [2])

$$\alpha\partial s = \frac{1}{p}\partial p - \frac{\gamma}{\rho}\partial\rho$$

which comes from

$$p/p_0 = e^{(s-s_0)/c_v}\left(\frac{\rho}{\rho_0}\right)^\gamma$$

with p_0, ρ_0 and s_0 reference states and c_v specific heat at constant volume. Note that since we are employing the chain rule we have implicitly assume that the flow is everywhere analytic, i.e. continuously differentiable. This is only true in the absence of shocks in the flow.

12

This leads to a rewritting of Eq. (5.1-3) as

$$\partial_t s + u \partial_x s = 0, \quad \text{or} \quad \frac{D}{Dt} s = 0 \qquad (5.1-4)$$

This implies that entropy is convected along steamlines. Flows which satisfy Eq. (5.1-4) are called isentropic. In the case of flows with shocks the entropy is constant along streamlines up to the shock, entropy jumps across the shock and then is constant along streamlines leaving the shock.

The next two equations (5.1-2b) and (5.1-2c) can be recombined if we assume isentropic, perfect gas. Then we use the relations $p = \kappa \rho^\gamma$, ($\kappa = p_0/\rho_0^\gamma$) and the perfect gas relation $c = \sqrt{\gamma p / \rho}$ which leads to

$$c = \sqrt{\gamma \kappa} \rho^{(\gamma-1)/2} \Rightarrow \frac{\partial \rho}{\rho} = \frac{2}{(\gamma-1)} \frac{\partial c}{c} \qquad (5.1-5a)$$

$$p = \kappa \rho^\gamma \Rightarrow \partial p = \frac{\gamma \kappa \rho^\gamma \partial \rho}{\rho} = \frac{\gamma p}{\rho} \partial \rho = c^2 \partial \rho \qquad (5.1-5b)$$

Then using Eq. (5.1-5), we have

$$\frac{\partial p}{\rho c} = c \frac{\partial \rho}{\rho} = \frac{2}{(\gamma-1)} \partial c \qquad (5.1-6)$$

We can now combine the partial derivatives in Eqs. (5.1-2b) and (5.1-2c) to give

$$[\partial_t + (u \pm c)\partial_x] (R^\pm) = 0 \qquad (5.1-7)$$

where we define the 1-D Riemann invariants $R^+ = u + 2c/(\gamma - 1)$ and $R^- = u - 2c/(\gamma - 1)$

The Riemann invariants are variables which are constant along the characteristic curves defined by $u \pm c$. These equations can be used in a initial value problem where given the initial state R_0^+ and R_0^- at time t = 0, we can then march along the characteristics to define values at later times and positions in space. This concept of marching along a characteristic direction is the underlying concept behind upwind characteristic schemes.

5.2 Flux Vector and Difference Splitting

In the last few years a number of schemes have been developed based on upwind differencing. The flux split schemes of Steger and Warming [4], Roe [8], and Van Leer [9] employ a decomposition of the flux vectors in such a way that each element can be stably differenced in an upwind fashion. Other schemes of a similar nature but based on complicated theories are the flux difference scheme of Osher and Chakravarthy [10] and Harten's TVD methods [11]. These schemes all claim (with

13

good justification) to be physically consistent since they follow in some sense the characteristics of the flow. They in general can be shown to produce sharp oscillation free shocks without added artificial dissipation. They are, though, complicated schemes which are just now being applied to complicated flowfield situations. Also it should be noted that these schemes have an inherent amount of internal dissipation, due to the one sided differences, which cannot be modified or decreased. For a more complete and recent look into upwind and TVD methods see Yee [12] and Van Leer, et. al. [13].

Steger - Warming Flux Splitting

The plus - minus flux split method of Steger and Warming [4] will be used here to introduce the concept of flux splitting. The approach taken is to split the eigenvalue matrix Λ of the flux Jacobians into two matrices, one with all positive elements and the other with all negative elements. Then the similarity transformations T_A or T_B are used to form new matrices A^+, A^- and B^+, B^-. Formally,

$$A = T_A \Lambda_A T_A^{-1} = T_A(\Lambda_A^+ + \Lambda_A^-)T_A^{-1} = A^+ + A^- \qquad (5.2-1)$$

with

$$\Lambda_A^\pm = \frac{\Lambda_A \pm |\Lambda_A|}{2} \qquad (5.2-2)$$

Here, $|\Lambda|$ implies that we take the absolute values of the elements of Λ. The two matrices, A^+ and A^- have by construction all positive and all negative eigenvalues, respectively.

New flux vectors can be constructed as

$$E = AQ = (A^+ + A^-)Q = E^+ + E^-, \quad F = BQ = (B^+ + B^-)Q = F^+ + F^- \qquad (5.2-3)$$

The Euler equations can now be written

$$\partial_t Q + \partial_x E^+ + \partial_x E^- + \partial_y F^+ + \partial_y F^- = 0 \qquad (5.2-4)$$

Different type of spatial differencing can now be used for each of the above flux vector derivatives. In the case of the $+$ terms a backward difference in space can be used (forward difference for the $-$ terms) and as discussed in Section 4.5, the resulting scheme maintains linear stability for the resulting ODE.

A generalized flux vector can be defined as

$$\widehat{F} = T_\kappa \widehat{\Lambda} T_\kappa^{-1} Q \qquad (5.2-5a)$$

where

$$\widehat{\Lambda}_A = \begin{bmatrix} \widehat{\lambda}_1 & & & \\ & \widehat{\lambda}_2 & & \\ & & \widehat{\lambda}_3 & \\ & & & \widehat{\lambda}_4 \end{bmatrix}, \qquad (5.2-5b)$$

14

with $\widehat{\lambda}$ any definition of an eigenvalue.

For example, we can have $\lambda^{\pm}$ from Eq. (5.2-2) to get $F^{\pm}$, or we could use $\widehat{\lambda}_i = u\}i = 1, 2, 3, 4$ producing a F^u and $\widehat{\lambda}_i = 0\}i = 1, 2$ with $\widehat{\lambda}_3 = c$, $\widehat{\lambda}_4 = -c$ producing a F^c. Note that then $E = F^u + F^c$.

The generalized flux vector, see Steger and Warming [4], is written as

$$\widehat{F} = \frac{\rho}{2\gamma} \begin{bmatrix} 2(\gamma - 1)\widehat{\lambda}_1 + \widehat{\lambda}_3 + \widehat{\lambda}_4 \\ 2(\gamma - 1)\widehat{\lambda}_1 u + \widehat{\lambda}_3(u + c\widetilde{\kappa}_x) + \widehat{\lambda}_4(u - c\widetilde{\kappa}_x) \\ 2(\gamma - 1)\widehat{\lambda}_1 v + \widehat{\lambda}_3(v + c\widetilde{\kappa}_y) + \widehat{\lambda}_4(v - c\widetilde{\kappa}_y) \\ f_1 \end{bmatrix} \qquad (5.2 - 6a)$$

where $f_1 = (\gamma - 1)\widehat{\lambda}_1(u^2 + v^2) + \widehat{\lambda}_3[(u + c\widetilde{\kappa}_x)^2 + (v + c\widetilde{\kappa}_y)^2]/2 + \widehat{\lambda}_4[(u - c\widetilde{\kappa}_x)^2 + (v - c\widetilde{\kappa}_y)^2]/2 + (3 - \gamma)(\widehat{\lambda}_3 + \widehat{\lambda}_4)c^2/(2(\gamma - 1))$ and

$$\widehat{\lambda}_1 = \widehat{\lambda}_2 = \kappa_x u + \kappa_y v, \quad \widehat{\lambda}_3 = \widehat{\lambda}_1 + c\sqrt{\kappa_x^2 + \kappa_y^2}, \quad \widehat{\lambda}_4 = \widehat{\lambda}_1 - c\sqrt{\kappa_x^2 + \kappa_y^2} \quad (5.2 - 6b)$$

The original E and F can be recovered with the appropriate values of κ_x and κ_y.

There is a very fundamental consideration pretaining to the flux vectors defined above. In the case of the $\pm$ flux splitting and other splitting which are a direct result of the similarity transform, Eq. (5.2-5), it is more often the rule then the exception that the flux Jacobians of the resulting flux vectors are not equal to the similarity matrices, i.e.

$$\frac{\partial F^{\pm}}{\partial Q} \neq A^{\pm} \qquad (5.2 - 7)$$

We shall not write out the exact Jacobians here, but we should note that for the $\pm$ splitting it has been shown that the eigenvalues of the exact Jacobians, while not $\Lambda^{\pm}$, are positive and negative appropriately for the $+$ and $-$ fluxes.

Van Leer Flux Splitting

In the Steger - Warming $\pm$ flux splitting if $u/c > 1$ then $F = F^+$ and $F^- = 0$. With the definition of $\Lambda^{\pm}$ given in Eq. (5.2-2) the split fluxes are continuous but not differentiable at sonic and stagnation points (due to the use of the absolute value and the discontinuous nature of the λ). This results in small local errors near the stagnation and sonic points. Steger and Warming [4] and Buning and Steger [14] suggest some remedies for this in which the λ are blended smoothly into their zero's. Van Leer [9] has developed a splitting in which he imposed a requirement that $\partial F^{\pm}/\partial Q$ must be a continuous function of the Mach number.

The generalized form for subsonic flow ($|U| < c$) is given in Van Leer [9] as

$$\widehat{F}^{\pm} = \begin{bmatrix} f_1^{\pm} \\ f_1^{\pm}[\widetilde{\kappa}_x(-U \pm 2c)\gamma + u] \\ f_1^{\pm}[\widetilde{\kappa}_y(-U \pm 2c)\gamma + v] \\ f_4^{\pm} \end{bmatrix} \qquad (5.2 - 8)$$

with

$$f_1^{\pm} = \frac{\pm \rho c}{4} \left(\frac{U}{c} \pm 1 \right)^2 \qquad (5.2 - 9a)$$

$$f_4^{\pm} = f_1^{\pm} \left(\left[\frac{-(\gamma - 1)U^2 \pm 2(\gamma - 1)Uc + 2c^2}{\gamma^2 - 1} \right] + \frac{u^2 + v^2}{2} \right) \qquad (5.2 - 9b)$$

where $U = \widetilde{\kappa}_x u + \widetilde{\kappa}_y v$. For supersonic flow , $F^+ = F$, $F^- = 0$ if $U \geq c$ and $F^+ = 0$, $F^- = F$ if $U \leq c$.

The Van Leer splitting is incorporated in the Euler equations just as in the Steger - Warming case. Equation (5.2-4) can be used and the appropriate differencing employed as before.

5.3 Flux Difference Splitting

In the flux vector split forms described above, we took a linear algebra approach to defining the equation sets. The flux vectors are split into seperate terms each of which satisfy certain predetermined properties which allow us then to choose appropriate diffencing schemes. An alternate approach is to employ flux difference splitting in which the equations are cast in difference form first and then appropriate splittings are applied to define the terms. Since we are not going deeply into numerical differencing schemes here, we shall restrict ourselves to assume that what is needed is a flux gradient at a cell interface when we attempt to balance fluxes to produce the desired scheme. Therefore we assume that on either side of the interface we have differing states of Q, i.e. Q_l (the left state) and Q_r (the right state). We then seek $\Delta F = F(Q_r) - F(Q_l)$ which is the flux gradiant across the interface.

There are a number of ways to determine ΔF, one could just form it from the definition of F applied at the two states and difference. We could also attempt to obtain ΔF by assuming constant states on either side of the interface and either solving the Riemann problem exactly, Eq. (5.1-7), or use approximate Riemann solvers such as suggested by Godunov [15], Osher and Solomon [16] , Harten, Lax, and Van Leer [17] or Roe [18]. Here we shall present Roe's approximate Riemann solver which is the most widely used because of its simplicity and efficiency.

Roe [18] defines the flux interface gradiant as

$$\Delta F = F(Q_r) - F(Q_l) = A(\overline{Q})(Q_r - Q_l) \qquad (5.3 - 1)$$

where $\overline{Q}$ is a nonlinear function of the left and right states. The requirements Roe applied are that $A(\overline{Q})$ has a complete set of eigenvalues and eigenvectors, that if $Q_l = Q_r$ then $A(\overline{Q}) = A(Q_l) = A(Q_r)$ and that the velocities lie between the left and right values. The Roe variables can be obtained from Q_l, Q_r by using

$$\overline{\rho} = \sqrt{\rho_l \rho_r}, \quad \overline{h} = \frac{\sqrt{\rho_l} h_l + \sqrt{\rho_r} h_r}{\sqrt{\rho_l} + \sqrt{\rho_r}}, \quad \overline{u} = \frac{\sqrt{\rho_l} u_l + \sqrt{\rho_r} u_r}{\sqrt{\rho_l} + \sqrt{\rho_r}} \qquad (5.3 - 2)$$

16

Once ΔF is defined in terms of the Roe Riemann solver, any number of upwind algorithms can be employed, see Yee [12] or Van Leer et.al. [13] for a good review. Additional to the upwind scheme one can add the constraint of TVD (total variation diminishing), Harten [11] which guarantees oscillation free solutions. Recently, higher order accurate schemes can such as ENO (essentially non oscillatory), Harten and Osher[19], symmetric TVD, Yee [12], and others, e.g. Osher and Chakravarthy [10] have been developed and represent the state of the art in this area.

VI. Vorticity and Entropy

The Euler equations govern the flow of inviscid fluid and therefore the only mechanism for the generation of vorticity is through shock waves. We can examine the Crocco - Vazonski equation (see Thompson [2] for a derivation)

$$\frac{D\Omega}{Dt} + (\Omega \cdot \nabla)\mathbf{u} - \Omega(\nabla \cdot \mathbf{u}) + \nabla T \times \nabla s = 0 \tag{6.1}$$

with $\Omega = \nabla \times \mathbf{u}$ the vorticity, $\mathbf{u}$ the velocity vector, ∇ the vector gradient operator and T temperature.
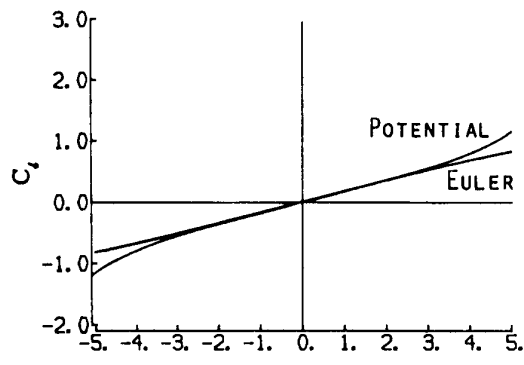
In the case of a homentropic flow $\nabla s = 0$, (constant entropy throughout the flow), a flow field with no initial vorticity $\Omega_0 = 0$ cannot generate vorticity since then $D\Omega/Dt = 0$. In flows with shocks ∇T and ∇s may not be zero and vorticity can be generated. In some flow problems we may introduce vorticity through the initializtion of the flow (a vortex may be introduced, see Srinivasan et.al. [20]) or through boundary conditions. In those cases, the Euler equations are very capable of accurately convecting and interacting the vorticity in the flow. In other cases, as we shall see below, vorticity may be created as a result of a shock in the flow or it may result from error in the computational technique. Usually we attempt to eliminate all of the computational errors, although it may not always be possible since all numerical schemes for the Euler equations require some level of artificial dissipation and dissipation is another mechanism for creating vorticity. When vorticity is generated as a result of a shock in the flow, the Euler equations (as we shall see) may produce solutions which convect vorticity and create flow structures which are usually associated with viscous flow. These solutions are valid, accurate solutions to the Euler equations and any or may not have physical significance.

17

VII. Applications
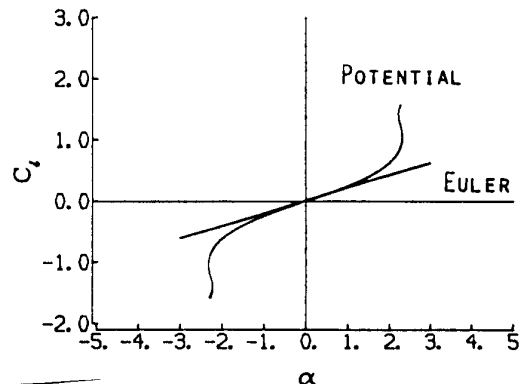
7.1 Perspectives To the Potential Equation

The conservative full potential equation is the current computational design tool used in industry. This is mainly because the solution algorithms and codes are usually more efficient and accurate (within the framework of the full potential approximation) than available Euler techniques. However, this is no longer necessarily the case in view of recent advances for the Euler equations such as multigrid codes, Jameson [21], direct solvers, Giles and Drela [22], and computational resources.

The conservative full potential equation under certain restrictions is a subset of the Euler equations and solutions of the potential equation will satisfy the Euler equations. This does not necessarily mean that the resulting solutions will be meaningful solutions for the physical situation. The Mach number limitation of the full potential equation is well known and understood. Salas and Gumbert [23] demonstrated in a landmark paper that although fixed point solutions (certain conditions) to the full potential equation can be accurate, the overall predictive quality of full potential result may be poor. In particular, they showed that trends such as lift-slope curves are incorrect relative to the Euler results. Results from Salas and Gumbert [23] are shown in Fig. 3 , here we show lift - slope curves for Euler and full potential solutions at two Mach numbers ($M_\infty = 0.67, 0.75$) for a NACA 0012 airfoil. They also demonstrate the possibility of nonuniqueness for full potential solutions for certain conditions and geometries and a corresponding lack of nonuniqueness for the Euler results.


Details of lift-curve for an NACA 0012 section at M_∞ = 0.67 computed with FLO 36 and FLO 52MG.

Details of lift-curve for an NACA 0012 section at M_∞ = 0.75 computed with FLO 36 and FLO 52MG.

FIGURE 3 LIFT - SLOPE CURVES FOR FULL POTENTIAL AND EULER SOLUTION.

A computational study which lends some insight into the efficiency and accu-

18

racy of Euler and full potential codes was performed by Flores et. al. [24]. Various Euler and full potential codes were compared in the transonic flow range for accuracy using mesh refinement and different grid generation techniques. The study also provided information on computational efficiency in terms of error versus CPU time. Results for a NACA 0012 airfoil at a subcritical Mach number, $M_\infty = 0.63$ and angle of attack, $\alpha = 2.0°$ are shown in Fig. 4. Figure 5 shows results for a NACA 0012 airfoil at a Mach number, $M_\infty = 0.75$ and angle of attack, $\alpha = 1.0°$ which produces a shock on the upper surface. In both cases, the asymtotic lift versus mesh refinement (the number of points in the computations were varied such that the averaged surface mesh spacing decreased with refinement) is shown for two Euler codes (ARC2D [25] and FLO52 [26]) and two potential codes (TAIR [27] and FLO36 [28]). Also shown are results for meshes generated with different techniques, algebraic [29] and Laplacian [30]. In Fig. 4a, we see that all the methods produced a fairly consistent asymtotic value of lift which compares well with Locks [31] widely accepted exact solution. Figure 4b shows percentage error in lift coefficient versus CPU time for the two formulations where the potential codes typically require an order of magnitude less CPU time per case. This was surprisingly better then originally expected, since the full potential codes were at a much more advanced stage at that time. Since then, the Euler codes have become more efficient and the current results would probably show the two methods closer together. The transonic case, Fig. 5, is obviously a case out of the range of validity for the full potential equation (the maximum Mach number gets too high), but the results are interesting nonetheless. The various methods still have consistent asymtotic values of lift, with the conservative full potential the highest, Fig. 5a. The CPU time comparison, Fig. 5b, shows less of a disparity between Euler and full potential formulations then the subcritical result. In this case since the error between full potential and Euler is large the results are for CPU time versus average mesh spacing. The full potential results typically require an unusual number of iterations in this range of conditions.

In general, the full potential equation (and subsequent codes) is a very useful and important tool in computational fluid dynamics and aerodynamics. A conclusion one might draw with respect to both the examples given above is that caution should be exercise in the choice of method applied to a particular problem. The full potential equation must be applied within a fairly restricted Mach number range and may not give proper incremental (trends) information. In contrast, Euler formulations may be more costly then a particular application warrants and care must be taken to decide where the dividing line lies.

7.2 Inviscid Airfoils

As an example of the capabilities of a typical Euler code results from the two - dimensional code ARC2D (developed at NASA Ames, Refs [25,32]) are presented for airfoil computations. The algorithm used in ARC2D is an implicit approximate factorization finite difference scheme which can be either first or second order ac-
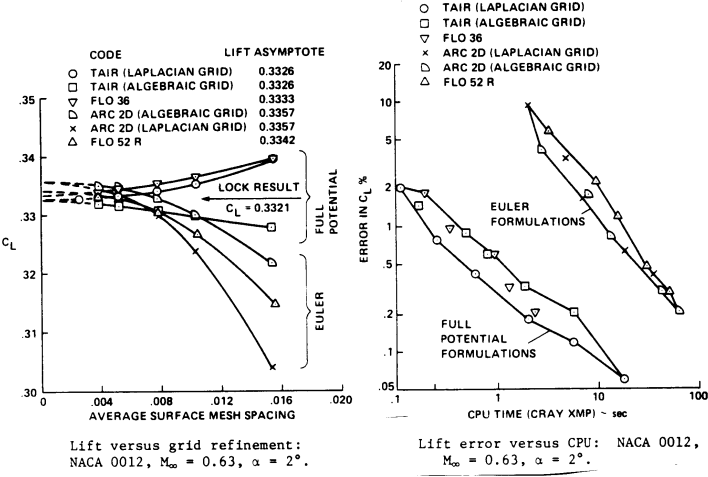
FIGURE 4. Subcritical Comparison Between Euler and Full Potential.
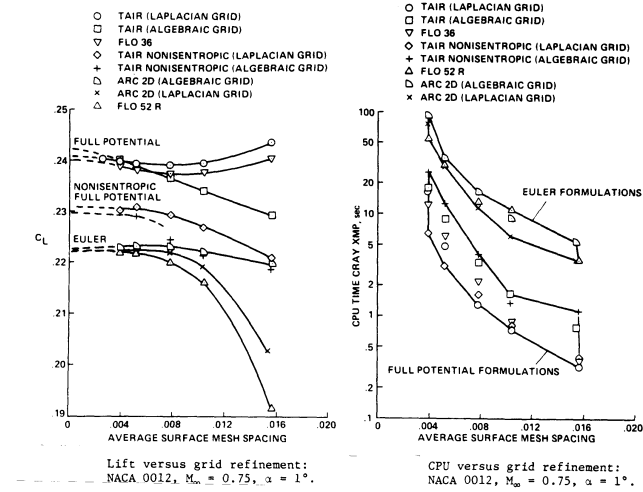
FIGURE 5. Transonic Comparison Between Euler and Full Potential.

curate in time. Local time linearizations are applied to the nonlinear terms and an approximate factorization of the two-dimensional implicit operator is used to produce locally one-dimensional operators. This results in block tridiagonal matrices, which are easy to solve. The spatial derivative terms are approximated with second order central differences. Explicit and implicit artificial dissipation terms are added to achieve nonlinear stability. A spatially variable time step is used to accelerate convergence for steady-state calculations. A diagonal form of the algorithm

20

is employed, Ref. [33], which produces a computationally efficient modification of the standard algorithm where the diagonalization results in scalar tridiagonal or pentadiagonal operators in place of the block operators. This diagonal form of the algorithm produces a robust, rapid, and versatile scheme for steady state calculations.

The ARC2D code has been applied to a wide variety of airfoil shapes, flow conditions, and other geometries. To demonstrate the accuracy and efficiency we have chosen two test cases, a NACA0012 airfoil at $M_\infty = 0.8$, $\alpha = 1.25°$ on a coarse grid (192 by 33 points) and a fine grid (248 by 49 points). For comparison purposes we use results from Jameson's multigrid Euler code FLO52R [26]. FLO52R is an Euler code using a multistage Runge-Kutta like algorithm with a multigrid scheme to accelerate convergence. The code employs enthalpy damping, residual averaging and an artificial dissipation model of the same form as used in ARC2D. The two codes were run on the same machine, the CRAY XMP at NASA Ames, on the same meshes and at the same flow conditions.

The first case is the NACA0012 airfoil at $M_\infty = 0.8$ and $\alpha = 1.25°$. The grid used is an "O" mesh topology with 192 points on the airfoil surface (running from the lower trailing edge around the nose to the upper trailing edge) and 33 point in the normal direction. The grid which is clustered at the leading and trailing edges, near the expected shock locations on the upper and lower surfaces and in the normal direction is shown in Fig. 6

Results from this case using ARC2D are shown in Fig. 7. We show here coefficient of pressure, Mach contours, pressure contours and contours of entropy. In Fig. 8 we show similar results for FLO52R. Computed lift for ARC2D is $C_L = 0.33957$ and for FLO52R $C_L = 0.32408$. The comparison between the two codes is quite good, despite the differences in spatial discretation.
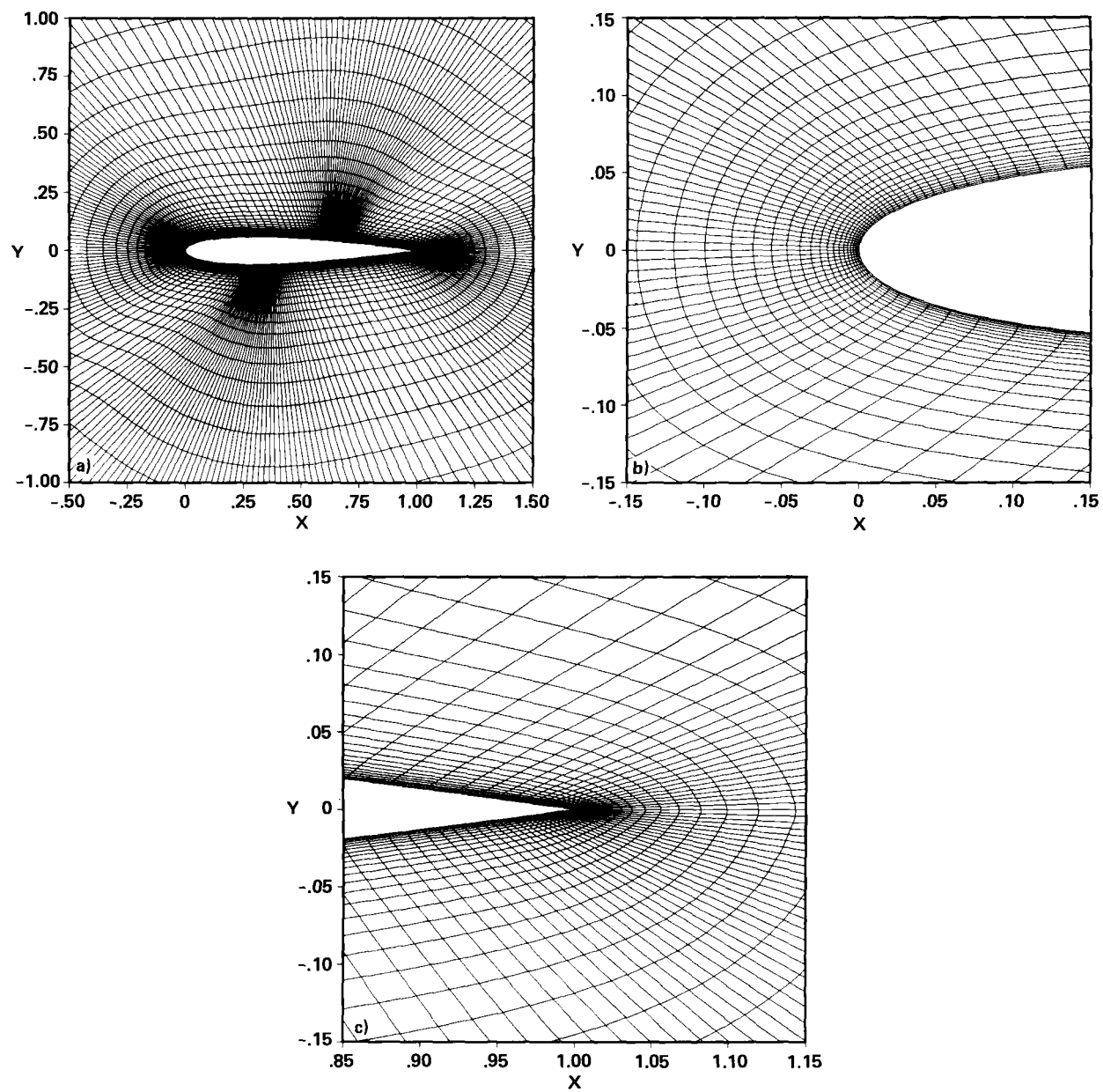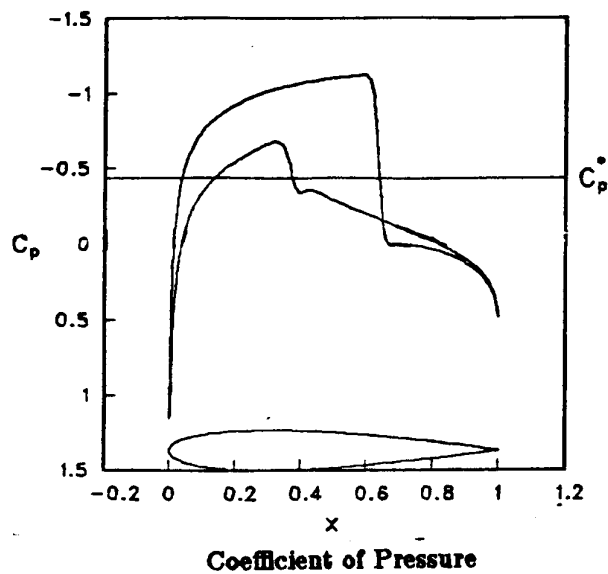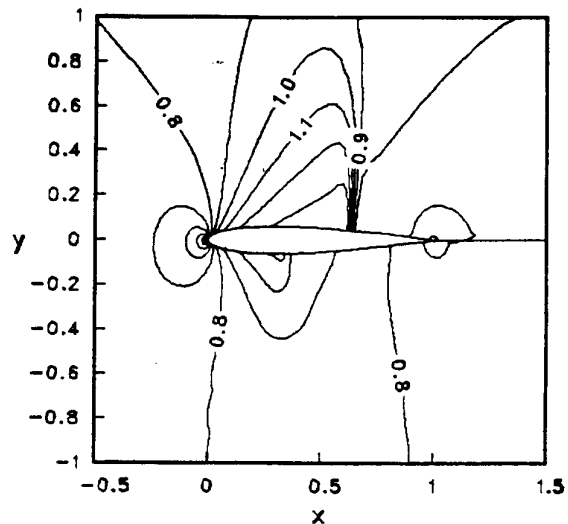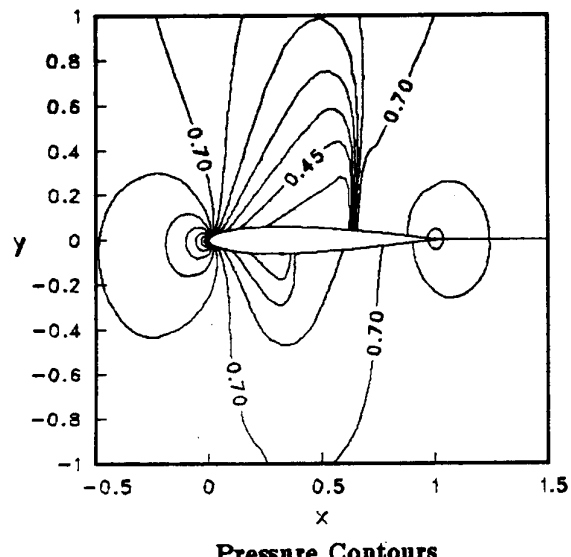
FIGURE 6. NACA0012 Grid Using 192 by 33 Grid Points.
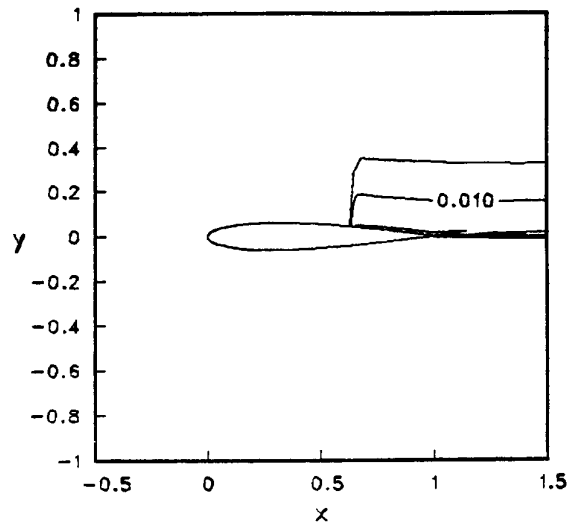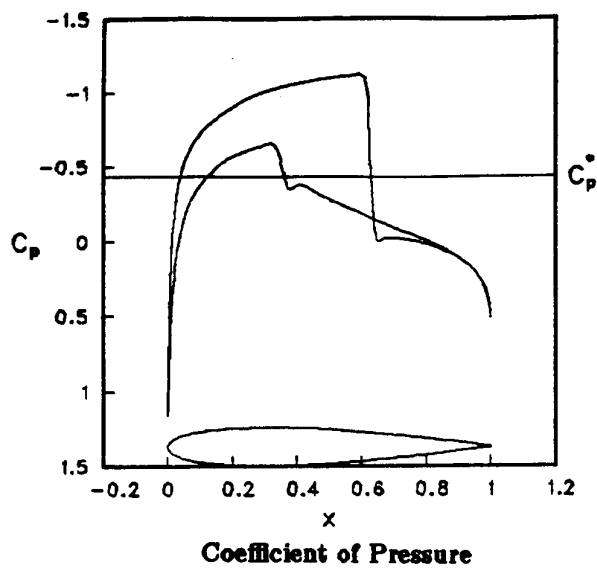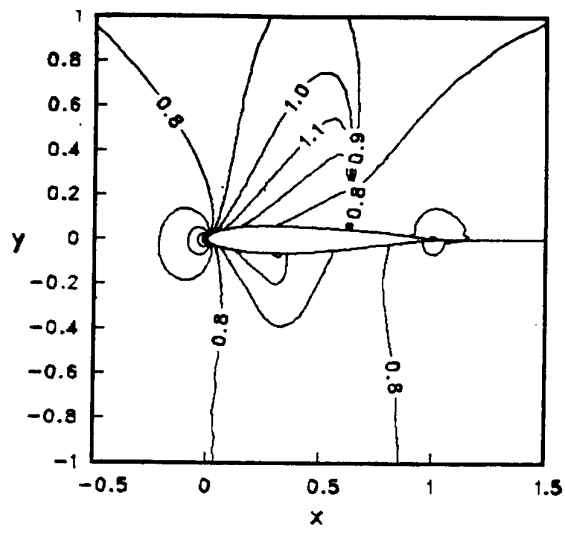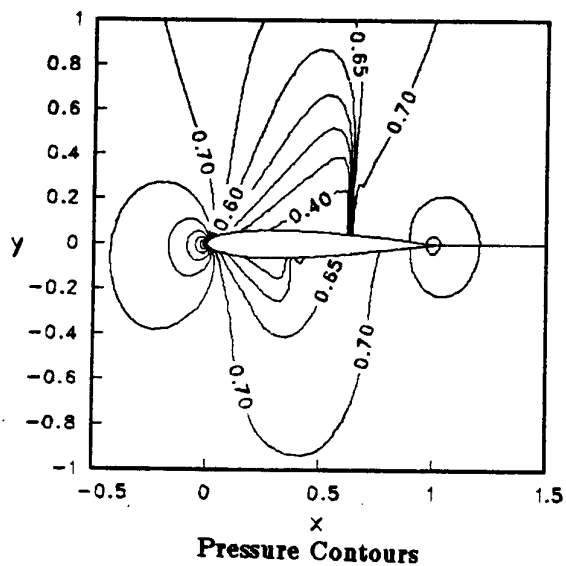
FIGURE 7. ARC2D Results for 192 by 33 Grid.

23
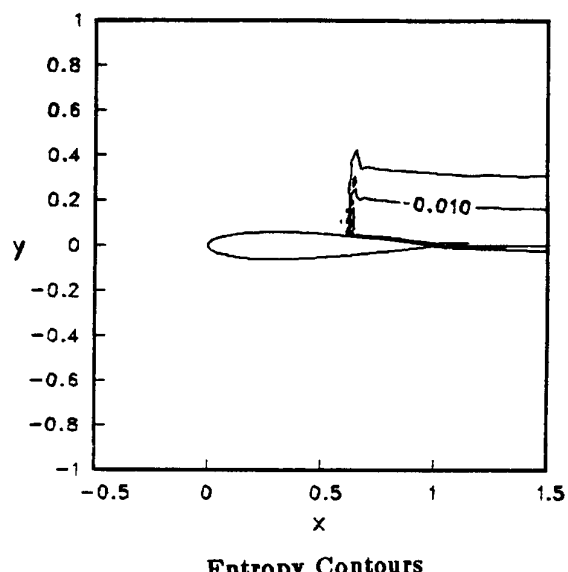
Coefficient of Pressure

Mach Contours

**Pressure Contours**

Entropy Contours

FIGURE 8.   FLO52R Results for 192 by 33 Grid.

We have established a number of accuracy checks and convergence criteria for comparison purposes. In terms of accuracy we recommend comparison of pressure coefficients, lift and other flow quantities. It is also important to establish the accuracy of certain flow regions. The stagnation region near the nose of the airfoil is particularly susceptible to errors due to poor boundary conditions, resolution, or physical assumptions. The best measure of this error is the entropy field. For inviscid flow there should be no generation of entropy at the leading edge of an airfoil in the absence of a leading edge shock. Examination of the entropy at the leading edge for the above case shows, see Fig. 9, that both codes give rise to some error at the leading edge, although the magnitude is rather small.
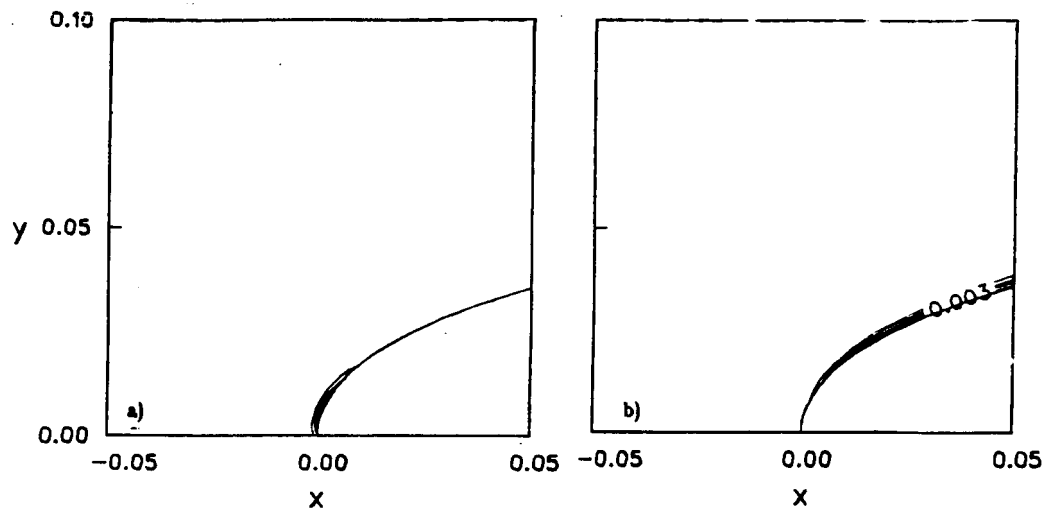

FIGURE 9. Entropy Errors at Leading Edge. a) ARC2D, b) FLO52R.

A number of convergence criteria have been chosen to assess the efficiency and convergence rates of the codes. We have chosen to use computer times as our measure of relative speed. Since the two codes are run on the same machines and with the same meshes this is an adequate measure. Other measures such as operation count, work or iteration are usually programming dependent or susceptible to misinterpretation. The convergence criteria used here are:

1. Coefficient of lift (C_L) to 1% of converged value.
2. Coefficient of lift (C_L) to 1/2% of converged value.
3. Coefficient of lift (C_L) to 5 decimal places.
4. Number of supersonic points to converged value.
5. Residual to machine zero. (10^{-13} on the Cray XMP.)

The residual is the l_2 norm of the steady state difference operator. We use just the component from the continuity equation, the other components behave similarly. For the above case on the 192 by 33 mesh the computer times for the convergence criteria are given in Table 1.

Convergence Comparison (seconds)		
Criteria	ARC2D	FLO52R
1% of C_L	6	8
1/2% of C_L	17	10.5
C_L to 5 places	57	31
No. S.S. pts	36	17
Machine zero	120	97

Table 1. Convergence Data for 192 by 33 grid.

As can be seen for this case FLO52R is up to twice as fast as ARC2D for some criteria. In either event these are fairly good convergence times. In general, these numbers carry over fairly consistently for a wide variety of airfoils and flow conditions for similar meshes.

A more stringent test is obtained with a finer grid and more grid points. A grid of 248 by 49 points is employed as the second study. The mesh is refined more at the nose, tail and near the shocks. Also to reduce the entropy errors at the nose the grid is clustered more tightly in the normal direction by reducing the minimum normal spacing by a factor of 2. The mesh is shown in Fig. 10.

Computational results for ARC2D and FLO52R are shown in Figs. 11 and 12. In this case the shocks are sharper and entropy errors at the leading edge are eliminated.

26
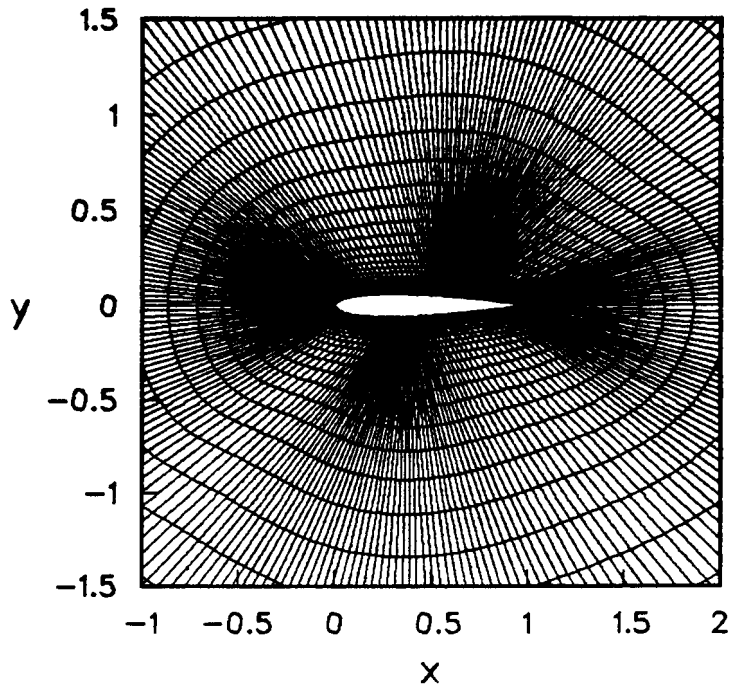
FIGURE 10. NACA0012 Mesh, 248 by 49.

Convergence data for this case is contained in Table 2. In Figure 13, we show convergence history vrs iteration for the two ARC2D results. All the results obtained with ARC2D were done using the fully implicit pentadiagonal algorithm. As mentioned above, numerous other cases and airfoils have been computed and perform similarly.

Convergence Comparison (seconds)		
Criteria	ARC2D	FLO52R
1% of C_L	38	23
1/2% of C_L	52.5	25.5
C_L to 5 places	174	168.5
No. S.S. pts	118	160
Machine zero	376	800+

Table 2. Convergence Data for 248 by 49 grid.

27

Coefficient of Pressure

Mach Contours

Pressure Contours

Entropy Contours
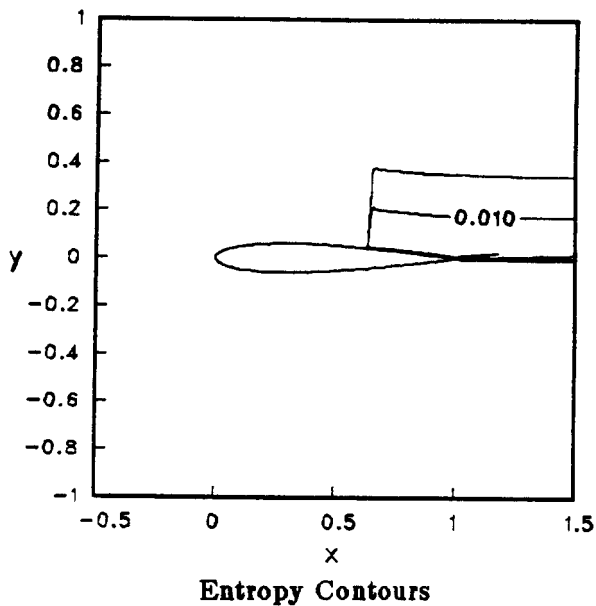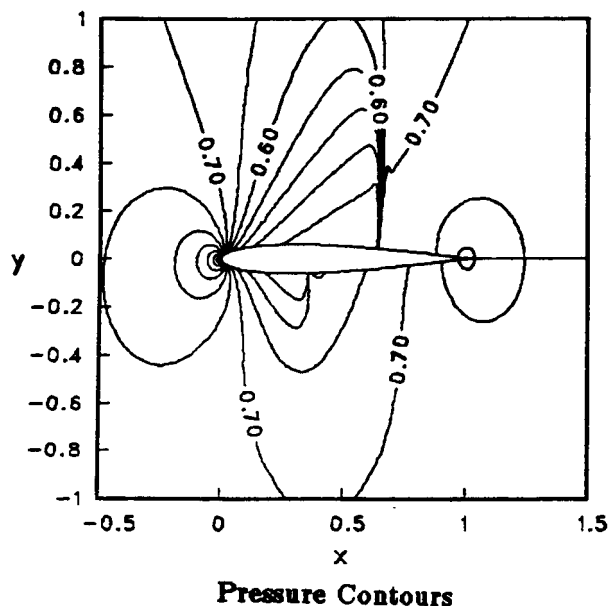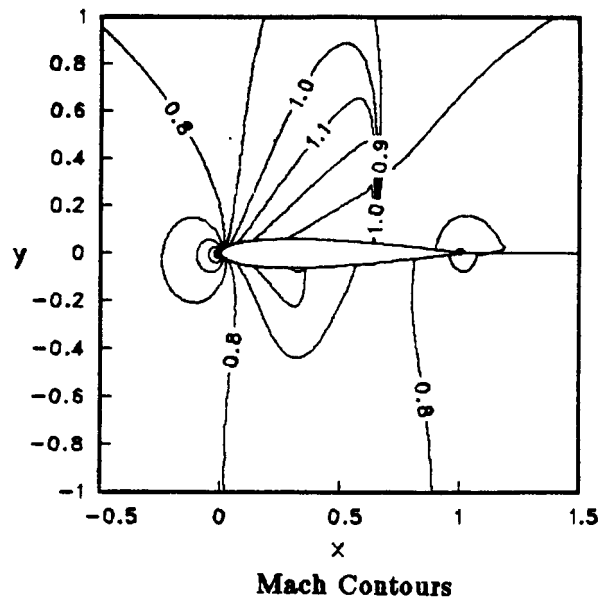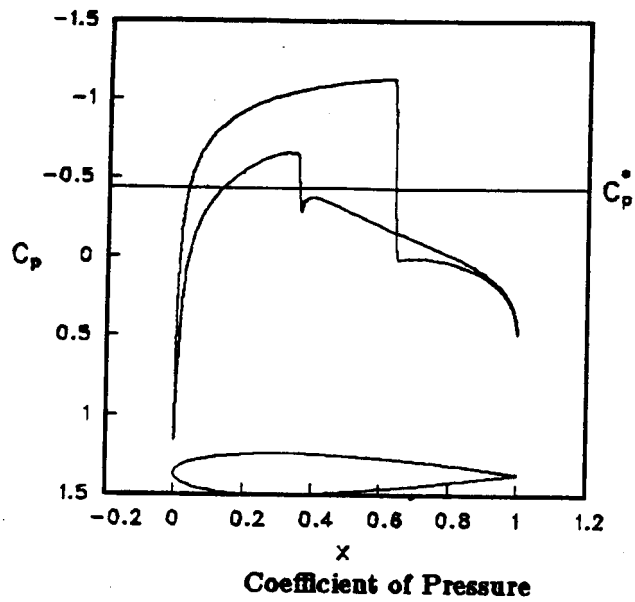
FIGURE 11. ARC2D Results for 248 by 49 Grid.

Coefficient of Pressure


Mach Contours

Pressure Contours


Entropy Contours
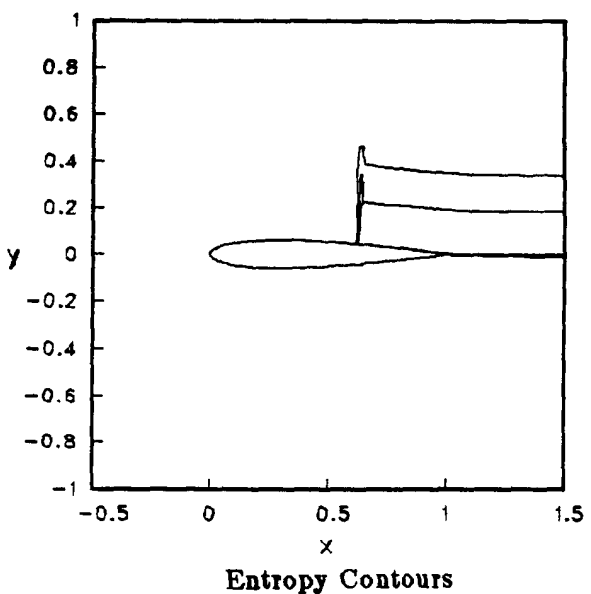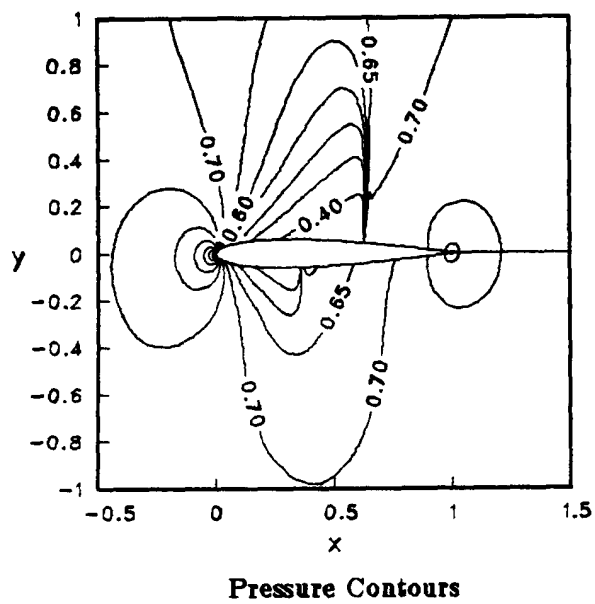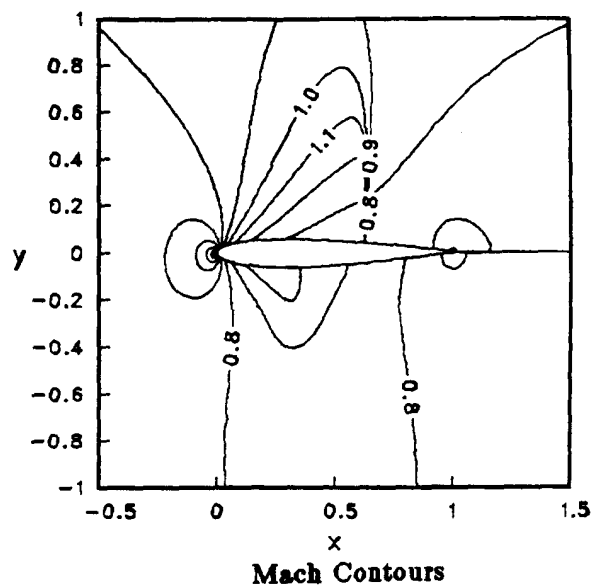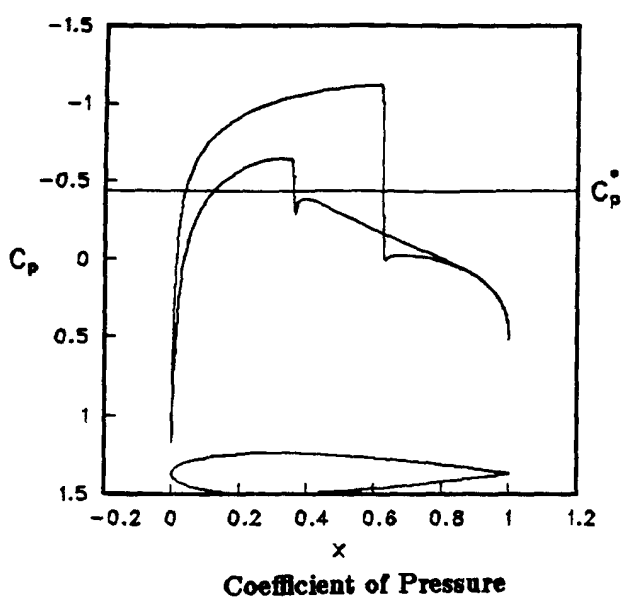
FIGURE 12. FLO52R Results for 248 by 49 Grid.

29
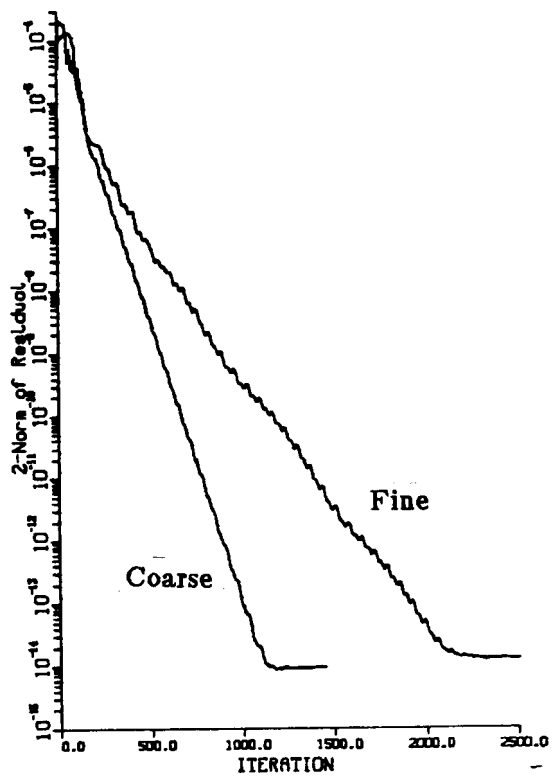
FIGURE 13. Convergence History vrs Iteration for ARC2D Results.

30

VII. Closing

The state of the art in the understanding and solution of the Euler equations is quite advanced. The newer schemes, (multigrid, direct solvers, TVD, ENO, etc) will provide us with many tools for obtaining high quality and efficient solutions for the Euler equations for a wide variety of flow conditions, geometries and physical problems. A word of caution is in order though. One must examine the application area to which the Euler equations are applied. It will always be possible to obtain a solution to the equations with varying degrees of accuracy where we will have exact solutions to the difference approximation for the continuous equations which in the limit of mesh refinement converges to the PDE solution. In some instances though, the solution obtained with the Euler equations will be far from the physically realizable solution. In that case, the Navier- Stokes equations must be solved.

References

1 Liepmann, H.W. and Roshko, A. *Elements of Gas Dynamics* ,New York,John Wiley & Sons, Inc., 1957

2 Thompson, P.A. *Compressible- FLuid Dynamics* ,New York, McGraw-Hill Book Company, 1972

3 Beam, R. and Warming, R. F. *An Implicit Finite-Difference Algorithm for Hyperbolic Systems in Conservation Law Form* **J. Comp. Phys.** Vol. 22 1976, pp. 87-110

4 Steger J. L. and Warming, R. F. *Flux Vector Splitting of the Inviscid Gas Dynamic Equations with Applications to Finite Difference Methods* **J. Comp. Phys.** Vol. 40 pp. 263-293 1981

5 Vinokur, M. *An Analysis of Finite- Difference and Finite- Volume Formulations of Conservation Laws* NACA CR 177416, 1986

6 Warming, R. F., Beam, R., and Hyett, B. J. *Diagonalization and Simultaneous Symmetrization of the Gas-Dynamic Matrices* **Math Comp** Vol. 29 1975 Page 1037

7 Steger, J. *Coefficient Matrices for Implicit Finite Difference Solution of the Inviscid Fluid Conservation Law Equations* **Computer Methods In Applied Mechanics and Engineering** Vol. 13 pp. 175-188 1978

8 Roe, P. L. *The Use of the Riemann Problem in Finite Difference Schemes,* **presented at the Seventh International Conference on Numerical Methods in Fluid Dynamics**, Stanford, CA 1980

9 van Leer, B. *Flux-Vector Splitting for the Euler Equations,* Eighth International Conference on Numerical Methods in Fluid Dynamic, Springer Lecture Notes in Physics no. 170, ed. E. Krause 1983

10 Osher S. and Chakravarthy, S. *Upwind Schemes and Boundary Conditions with Applications to Euler Equations in General Geometries,* **J. Comp. Phys.** Vol.

50 pp. 447–481 1983

11   Harten, A. *A High Resolution Scheme for the Computation of Weak Solutions of Hyperbolic Conservation Laws* **J. Comp. Phys.** Vol. 49 1983 pp. 357-393

12   Yee, H. —*Upwind and Symmetric Shock Bapturing Schemes*, NASA TM 89464, 1987

13   Van Leer, B., Thomas, J.L., Roe, P.L., and Newsome, R.W. *A Comparison of Numerical Flux Formulas for the Euler and Navier- Stokes Equations,***AIAA Paper 87-1104**,AIAA 8th Computational Fluid Dynamics Conference, Honolulu, Hawaii., 1987, pp.357-393

14   Buning, P. and Steger, J.L., *Solution of the Two- Dimensional Euler Equations with Generalized Coordinate Transformation Using Flux Vector Splitting,***AIAA Paper 82-0971**, AIAA/ASME 3rd Joint Thermophysics, Fluids, Plasma and Heat Transfer Conference, St. Louis, Mo, 1982

15   Godunov, S.K.,*A Finite Difference Method for the Numerical Computation of Discontinuous Solutions of the Equations of Fluid Dynamics*, **Mat. Sh.** , Vol 47, pp. 357-393, 1959

16   Osher, S. and Solomon, F.,*Upwind Difference Schemes for Hyperbolic Systems of Conservation Laws*, **Math. Comp.**, Vol 38, pp. 339-374,1982

17   Harten, A., Lax, P.D. and Van Leer, B.,*On Upstream Differencing and Godunov-Type Schemes for Hyperbolic Conservation Laws* **SIAM Rev.**, Vol 25, pp. 31-61, 1983

18   Roe, P. L. *Approximate Riemann Solvers, Parameter Vectors, and Difference Schemes,*, **J. Comp. Phy.**, Vol 43, pp. 357-372, 1981

19   Harten, A. and Osher, S. *Uniformly High- Order Accurate Nonoscillatory Schemes*, **SIAM J. Num. Anal.** Vol 24, No.2 ,pp. 279-309 , 1987

20   Srinivasan, G., McCroskey, W.J., and Kutler, P.. *Numerical Simulation of the Interaction of a Vortex with Stationary Airfoil in ransonic Flow* , **AIAA Paper 84-0254**,AIAA 22nd Aerospace Sciences Meeting, Reno, Nv , 1984

21   Jameson, A. *Successes and Challenges in Computational Aerodynamics* , **AIAA Paper 87-1184**, AIAA 8th Computational Fluid Dynamics Conference, Honolulu, Hawaii , 1987

22   Giles, M.B. and Drela, M. *A Two- Dimensional Transonic Aerodynamic Design Method* , **AIAA Paper 86-1973**,AIAA 4th Aerodynamics Conference, San Diego, Ca , 1986

23   Salas, M.D. and , Gumbert, C.R. *Breakdown of the Conservative Potential Equation* , **AIAA Paper 85-0367**, AIAA 23nd Aerospace Sciences Meeting, Reno, Nv , 1985

24   Flores, J., Barton, J., Holst, T. and Pulliam, T. *Comparison of the Full Potential and Euler Formulations*, For Computing Transonic Airfoil Flows Presented at the 9th International Conference on Numerical Methods in Fluid Dynamics, Saclay, France, June 1984 , **Lecture Notes in Physics**, Vol 218, No. 5 Editor

Soubbaramayer and J. Boujot, Springer-Verlag, 1985

25   Pulliam T. H. and Steger, J. L. *Recent Improvements in Efficiency, Accuracy, and Convergence for Implicit Approximate Factorization Algorithms* , **AIAA Paper 85-0360**, AIAA 23rd Aerospace Sciences Meeting, Reno, Nev., Jan. 1985

26   Jameson, A., Schmidt, W. and Turkel, E. *Numerical Solutions of the Euler Equations by Finite Volume Methods Using Runge- Kutta Time-* Stepping *Schemes* , **AIAA paper 81-1259**, AIAA 14th Fluid and Plasma Dynamics Conference, Palo Alto , 1981

27   Holst, T. L. *Implicit Algorithm for the Conservative Transonic Full-Potential Equation Using an Arbitrary Mesh* , **AIAA J. 17**, 1979 ,pp. 1038–1045

28   Jameson A. *Acceleration of Transonic Potential Flow Calculations on Arbitrary Meshes by the Multiple Grid Method* , **AIAA Paper 79-1458**,1979

29   Eiseman, P. *Geometric Methods in Computational Fluid Dynamics* **ICASE Report 80-11** , 1980

30   Thompson, J. , Thames, F. and Mastin, C. *Automatic Numerical Generation of Body Fitted Curvilinear Coordinate Systems for Field Containing Any Number of Arbitrary Two Dimensional Bodies,* **J. Comp. Phy.** Vol 15 ,pp. 299-319 , 1974

31   Lock, R.C. *Test Cases for Numerical Methods in Two- Dimensional Transonic Flows,* **AGARD Report No. 575** , 1970

32   Pulliam, T. H. *Euler and Thin Layer Navier Stokes Codes : ARC2D, ARC3D,* Computational Fluid Dynamics, A workshop Held at the University of Tennessee Space Institute, UTSI publ. E02-4005-023-84, 1984

33   Pulliam T. H. and Chaussee D. S. *A Diagonal Form of an Implicit Approximate Factorization Algorithm,* **Journal of Computational Physics**, Vol 39 , 1981